Journal of Alloys and Compounds 509 (2011) 936–941

Contents lists available at ScienceDirect

Journal of Alloys and Compounds

journal homepage: www.elsevier.com/locate/jallcom

Sol–gel derived (Li, Ta, Sb) modified sodium potassium niobate ceramics: Processing and piezoelectric properties

Hongqiang Wang, Ruzhong Zuo*, Jian Fu, Yi Liu

Institute of Electro Ceramics & Devices, School of Materials Science and Engineering, Hefei University of Technology, Hefei 230009, PR China

ARTICLE INFO

Article history:
Received 11 August 2010
Received in revised form
10 September 2010
Accepted 18 September 2010
Available online 29 September 2010

Keywords:
Sol–gel
Ceramics
Ferroelectrics
Piezoelectricity

ABSTRACT

Nano-scaled lead-free perovskite powders (50–100 nm) with a composition of $(Na_{0.52}K_{0.4425})(Nb_{0.8825}Sb_{0.08})O_3-0.0375LiTaO_3$ (NKNS-3.75LT) have been synthesized via a modified low-cost citrate sol–gel route, in which Nb_2O_5 and Ta_2O_5 were transformed into stable and soluble chelate complexes to replace costly metal alkoxides. The thermal decomposition process and structural transformation behavior of the as-prepared xerogel was investigated by means of thermo-gravitometry and differential scanning calorimetry, X-ray diffractometry and Fourier-transform infrared spectrometry. The results indicated that the ideal crystallization of the NKNS-3.75LT powder with a single perovskite structure occurs at 500–600 °C, significantly lower than that for a conventional mixed-oxide route. Transmission electron microscopy observation showed that the crystalline powder has particle sizes in the range of 30–100 nm and exhibits polyhedron-like morphology, probably resulting in a specific grain growth behavior upon densification. The sol–gel derived NKNS-3.75LT ceramics sintered at 1090 °C exhibit excellent piezoelectric properties of d_{33} ~418 pC/N and k_p ~0.54 for NKN based random ceramics.

1. Introduction

Lead-free piezoelectric ceramics have attracted a lot of attention in the last few years mainly owing to increasing concerns to the environment. As one important member of lead-free family, the $(Na,K)NbO_3$ (NKN) based lead-free compositions were extensively investigated [1–4] and have been considered as one of the most potential candidate materials based on their large piezoelectric constant d_{33} of >300 pC/N. Particularly, the (Li, Ta, Sb)-modified NKN ceramics were reported to have comparable piezoelectric properties to those of some commercial PZT ceramics [5–8]. The piezoelectric and electromechanical properties have been so far obviously modified through a lot of attempts to optimize the composition and processing [7–9], and to improve the thermal stability [4,9]. It can be found that most of these researches were focused on conventional solid-state reaction methods for making random NKN based piezoelectric ceramics. This traditional synthesis method usually needs relatively high calcination temperatures and sintering temperatures at which the evaporation of Na_2O and K_2O could become more serious. Moreover, complex compositions are difficult to get homogeneously distributed in a solid state reaction method [10,11], probably inducing difficulties of controlling the microstructure and chemical stoichiometry.

By comparison, soft-chemical routes exhibit outstanding advantages and have been widely used to prepare superfine powders and thin films. Some merits like accurate chemical stoichiometry, good composition homogeneity and low crystallization temperature can be achieved owing to the mixing of various liquid precursors on a molecular level. Such chemical methods as citrate method [12], conventional sol–gel method [13], hydrothermal method [14,15], mechanochemical synthesis [16] and sol–gel auto-combustion method [17,18] have been applied in recent years for sodium bismuth titanate based lead-free ceramics, leading to the improved densification behavior and electrical properties. Unfortunately, the soft-chemical route has not been extensively applied in NKN based ceramics, although it was occasionally used to make niobate based thin films [19–21], probably because metal alkoxides $(C_nH_{2n+1}O)_5Nb$ have made this processing costly in the preparation of the powders [22]. Only few attempts have been made to make Li-doped NKN powders by a sol–gel process using Nb_2O_5 as Nb source [23,24], in which the problem of easier hydrolysis of niobium alkoxides could be avoided. Unfortunately, this attempt has never been extended to the preparation of more complex compositions based on NKN as concluded from the literature survey. More noticeably, the processing and electrical properties of sol–gel derived (Li, Ta and Sb) modified NKN bulk ceramics have never been reported either.

The purpose of this study is thus to explore a modified citrate sol–gel process using Nb_2O_5 and Ta_2O_5 as niobium and tantalum sources to prepare typical lead-free piezoelectric ceramics

* Corresponding author. Tel.: +86 551 2905285; fax: +86 551 2905285.
E-mail address: piezolab@hfut.edu.cn (R. Zuo).

0925-8388/$ – see front matter © 2010 Elsevier B.V. All rights reserved.
doi:10.1016/j.jallcom.2010.09.134

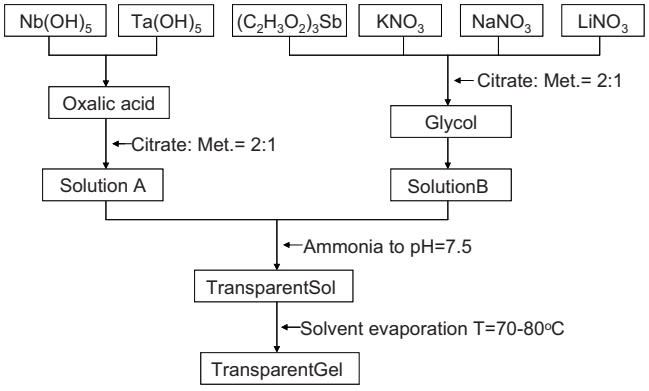

Fig. 1. Flow chart of preparing NKNS-3.75LT gel via a citrate sol–gel method.

of $(Na_{0.52}K_{0.4425})(Nb_{0.8825}Sb_{0.08})O_3-0.0375LiTaO_3$ (NKNS-3.75LT), which have been previously prepared by a mixed-oxide solid state method and exhibited excellent piezoelectric properties of d_{33} ~395 pC/N and k_p ~64% [8]. A special attention was focused on the chemical reaction condition and structural transformation behavior of the as-prepared xerogel by means of kinds of characterization techniques. Moreover, the sintering, microstructure and piezoelectric properties of the sol–gel derived NKNS-3.75LT ceramics have been discussed. The results are expected to extend the application of sol–gel routes to high-performance NKN-based lead-free ceramics with complex compositions.

2. Experimental procedure

The raw materials used in this study are Nb_2O_5 (≥99.5%), Ta_2O_5 (≥99.5%), K_2CO_3 (≥99.0%), $NaNO_3$ (≥99.0%), KNO_3 (≥99.0%), $LiNO_3$ (≥99.0%), glycol (≥99.0%), HNO_3 (65.0–68.0%), $Sb(CH_3COO)_2$ (≥99.9%), citric acid (≥99.5%), oxalic acid (≥99.5%) and ammonia (25–28%). Firstly, Nb_2O_5 and K_2CO_3 were mixed and calcined at 900 °C for 2 h to form a soluble potassium tantalate according to their phase diagram [25]. Then, the as-prepared potassium tantalate was dissolved in distilled water and titrated by nitric acid to obtain a precipitate of tantalum hydroxide by adjusting the pH value of the solution. Finally, the precipitate of tantalum hydroxide was washed and filtered over 10 times so as to make sure that K ions were totally removed. The relevant chemical reactions [26] can be written as follows:

$$Ta_2O_5 + 3K_2CO_3 = 2K_3TaO_4 + 3CO_2$$

$$6K_3TaO_4 + 5H_2O = 18K^+ + Ta_6O_{19}^{8-} + 10OH^-$$

$$Ta_6O_{19}^{8-} + 8H^+ + 11H_2O = 6Ta(OH)_5\downarrow$$

A similar preparation procedure was used to make niobium hydroxide. Both niobium precursor and tantalum precursors were chelated with citric acid. The NKNS-3.75LT gel was prepared following the procedure as indicated in Fig. 1. The molar ratio of citric acid to metal cations was 2:1. The niobium hydroxide and tantalum hydroxide were firstly dissolved in oxalic acid solution and then added with citric acid as chelating agent to form chelate complex with niobium ions and tantalum ions (solution A). According to the required stoichiometry, KNO_3, $NaNO_3$, $LiNO_3$ and $Sb(CH_3COO)_2$ were introduced into glycol (solution B). Subsequently, solution A and solution B were mixed to form a stable sol by adjusting the pH value to ~7.5. Citric acid is a polydentate ligand with three carboxyls and a hydroxyl and can easily form stable and soluble chelate complexes with metal cations in an alkalescent solution. Glycol with double hydroxyl groups can form ester groups and network structures by increasing molecular weight of precursors, and further enhance the stability of solution. The as-prepared sol was heated at 70–80 °C to remove redundant solvent and to form gel. In the end the xerogel was calcined at 200–800 °C for 3 h to obtain crystallite powders. The powder compact was then sintered in air within the temperature range of 1050–1130 °C at a heating rate of 5 °C/min.

Thermo-gravimetry (TG) and differential scanning calorimetry (DSC) analysis of the as-prepared gel was carried out using a simultaneous thermal analyzer (STA409C, Netzsch, Germany). The structure evolution of the gel after heat treatment was analyzed by a Fourier-transform infrared (FT-IR) spectrometer (Spectrum 400, PerkinElmer, USA). The powders calcined at different temperatures were characterized by an X-ray diffractometer (XRD, D/MAX2500 VL/PC, Rigaku, Japan), and a Raman spectrometer (LabRAM HR800, HJY, France). The morphology of the as-synthesized crystallite particles was analyzed by means of a transmission electron microscope (TEM, Model H-800, Hitachi, Japan). The microstructure on the surface

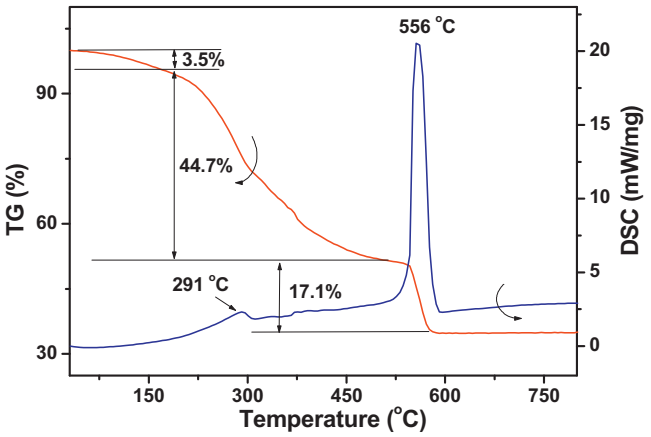

Fig. 2. Thermo-gravitometry and differential scanning calorimetry analysis of the NKNS-3.75LT gel.

of the ceramics sintered at different temperatures was observed using a scanning electron microscope (SEM, SSX-550, Shimadzu, Japan). The sample density was evaluated by the Archimedes method. The dielectric properties (dielectric constant ε_{33}^T and loss tanδ) were measured with changing temperature by an LCR meter (Agilent E4980A, USA). The piezoelectric constant d_{33} was measured directly on a quasi-static d_{33} meter (YE2730A, Sinocera, China). The electromechanical coupling coefficient k_p was measured by a high precision impedance analyzer (PV70A, Beijing Band ERA Co., Ltd. China). The remnant polarization (P_r) was characterized by measuring polarization versus electric field hysteresis loops using a ferroelectric measuring system (Precision LC, Radiant Technologies, Inc., USA).

3. Results and discussion

The TG and DSC curves of the NKNS-3.75LT gel are shown in Fig. 2. A small weight loss of 3.5% at temperatures up to ~150 °C is due to the evaporation of remaining water, glycol and ammonia. The exothermic peaks at ~291 °C could be attributed to the thermal decomposition of citrate complexes, corresponding to a weight loss of 44.7%. The strong exothermic peak at 556 °C would be related to the combustion of residual organic components, accompanied by a weight loss of 17.1%. No further weight loss or peaks can be seen thereafter in TG and DSC curves, indicating that the thermal decomposition of the NKNS-3.75LT gel or the removal of organic substances has been completed before 600 °C.

The thermal decomposition process of the xerogel can be analyzed in more details by room-temperature FT-IR spectra as shown in Fig. 3. The samples were prepared by calcining the xerogel at

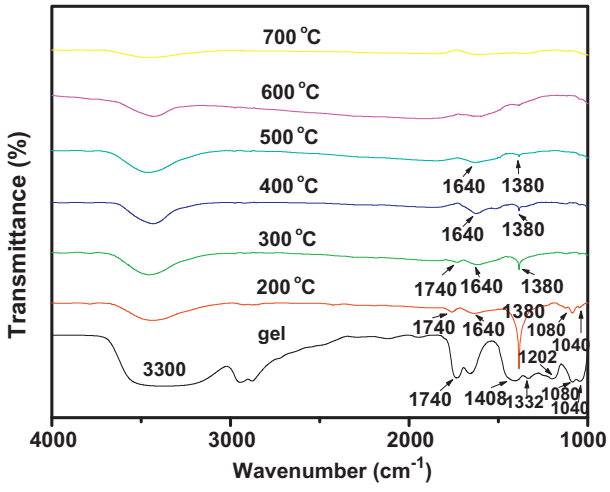

Fig. 3. Fourier-transform infrared spectra of the NKNS-3.75LT gel and as-calcined powders at different temperatures as indicated.

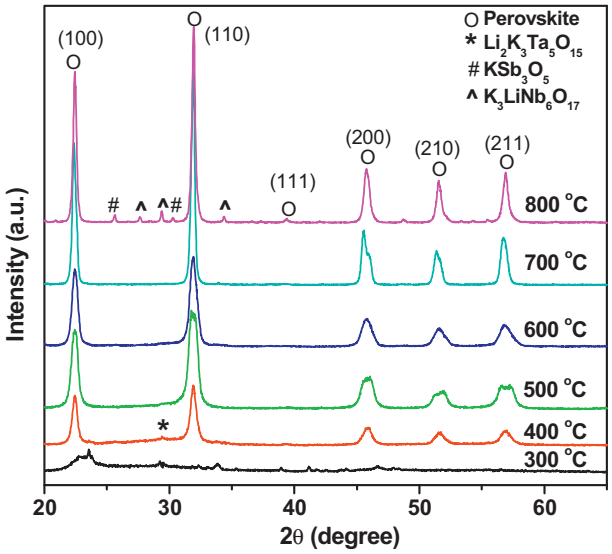

Fig. 4. X-ray diffraction patterns of the NKNS-3.75LT gel powders calcined at different temperatures as indicated.

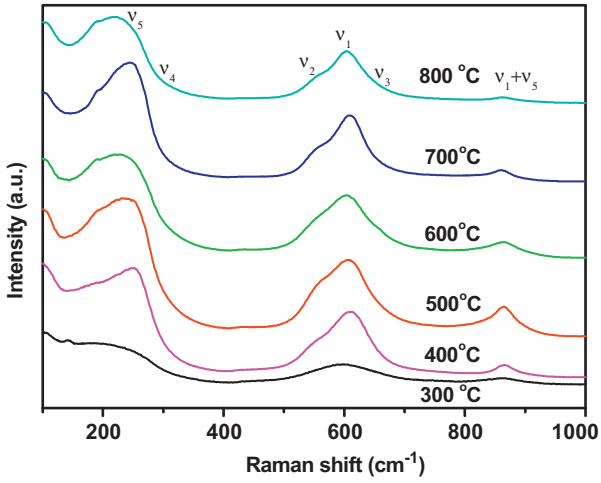

Fig. 5. Raman spectrum of the NKNS-3.75LT powders obtained by heat-treating the gel at different temperatures as indicated.

different temperatures. Peaks were assigned with reference to standard texts [27]. The broad absorption peak around 3300 cm^{-1} is typical of O–H stretching from H_2O. In the gel sample, the peaks at 1040 cm^{-1} and 1080 cm^{-1} are attributed to C–O stretching from remains of glycol. The peak at 1202 cm^{-1} is due to the vibration of –C–O–C– bonds between the acid and hydroxyl groups in citric acid and glycerol, which offers an evidence for the esterification during processing [28]. The peaks at 1332 cm^{-1} and 1408 cm^{-1} are ascribed to the symmetric vibration of $–COO^-$ from metal carboxylates, indicating that the chelation of metal ions exists [29]. It is thus concluded that in this study citric acid as a chelating agent was chelated with metal ions to form a stable network structure. After heat treatment, obvious changes happen in FI-IR spectra. The peaks at 1380 cm^{-1} can be assigned to CH_3 symmetric bending [22] related to inorganic carbonates or bicarbonates (HCO_3^-), indicating that citrate complexes decompose into carbonates between 200 °C and 300 °C. This reaction could be the reason for the exothermic peak at ~291 °C in the DSC curve. In addition, the presence of peaks at 1640 cm^{-1} and 1740 cm^{-1} can be attributed to the C=C and C=O stretching, respectively, suggesting the thermal decomposition of organic matters occurs. Before 500 °C, the absorption peaks are nearly the same, except that the absorption strength becomes weak with increasing temperature. Starting from 600 °C, there is no indication of organic residues from IR spectra but a weak absorbance in the O–H stretching (3300 cm^{-1}), assuming that all organic substances have been decomposed after 600 °C.

The crystallization behavior of the NKNS-3.75LT gel undergoing the treatment at different temperatures was characterized, as shown in Fig. 4. The powders exhibit typical patterns of amorphous phases below 300 °C. As the calcination temperature rises to 400 °C, the characteristic diffraction peaks of a perovskite structure begin to appear apart from a small amount of secondary phases (indexed as $Li_2K_3Ta_5O_{15}$). A single perovskite structure can be obtained till the gel was calcined at 500 °C. Between 500 °C and 700 °C, nothing happened except for slight changes in the crystal symmetry as seen from the splitting of (200) diffraction peaks. This could be attributed to the degree of grain growth and the particle size effect. That is to say, there exists a grain size induced phase transition from pseudocubic to orthorhombic phases, leading to the change of the phase content. However, powders calcined at 800 °C obviously contain secondary phases (indexed as $K_3LiNb_6O_{17}$ and KSb_3O_5), probably because of the volatilization of Na_2O and K_2O. Combined with TG-DSC analysis and IR spectra, it can be recognized that the sol–gel derived powders can be well synthesized at 600 °C, approximately 200–300 °C lower than those prepared by a conventional mixed-oxide method [2–4]. The homogeneous mixing of chelate complexes and metal cations at a molecular level provides the possibility for obviously reduced migration distance of various ions.

In order to deeply explore the phase structural transformation of the gel powders undergoing the heat treatment, Raman spectra of these powders at room temperature are shown in Fig. 5. As a main unit of a perovskite structure, the vibrations of the NbO_6 octahedra are usually considered to consist of $1A_{1g}(\nu_1)+1E_g(\nu_2)+2F_{1u}(\nu_3+\nu_4)+F_{2g}(\nu_5)+F_{2u}(\nu_6)$ [30], among which $1A_{1g}(\nu_1)+1E_g(\nu_2)+F_{1u}(\nu_3)$ belong to stretching modes and the other belong to bending modes. As shown in Fig. 5, the stretching and bending modes of NbO_6 octahedra start to appear in the sample which was heat treated at 400 °C, indicating the formation of perovskite structure. This is in good agreement with the XRD results (Fig. 4). However, owing to its low crystallinity, the intensity of Raman spectrum is low for the sample calcined at 400 °C. It can be seen that the intensity of Raman spectrum increases with an increase of the calcination temperature. Furthermore, the wavenumber of the ν_1 mode representing a double-degenerate symmetric O–Nb–O stretching vibration moves towards to higher value with increasing the calcination temperature. The same change trend is observed in the $\nu 5$ mode representing a triply degenerate symmetric O–Nb–O bending vibration. Similar to the XRD results, these changes could be related to the variation of crystallinity (Fig. 4) and grain size (see infra), which tends to induce a change of NbO_6 octahedra. A reduction in the intensity of Raman spectrum can be observed in the sample calcined at 800 °C, probably because of the presence of the secondary phase.

The particle morphology of the NKNS-3.75LT gel powders calcined at 500–800 °C for 3 h is shown in Fig. 6. It can be seen that the average particle size is about 30 nm for the powder calcined at 500 °C. However, the polyhedral particles clustered into the agglomeration, resulting from some residual organic substances between them. The existence of residual organic matters can be confirmed by the above-mentioned DSC-TG analysis. As the calcination temperature rises to 600 °C, most of particles are well dispersed with only a slight degree of soft agglomeration. The particle morphology is still polyhedral but the average particle size reaches 100 nm. The particles were obviously coarsened as the calcination temperature was further increased (~150 nm and ~200 nm for 700 °C and 800 °C, respectively). However, the rapid grain growth

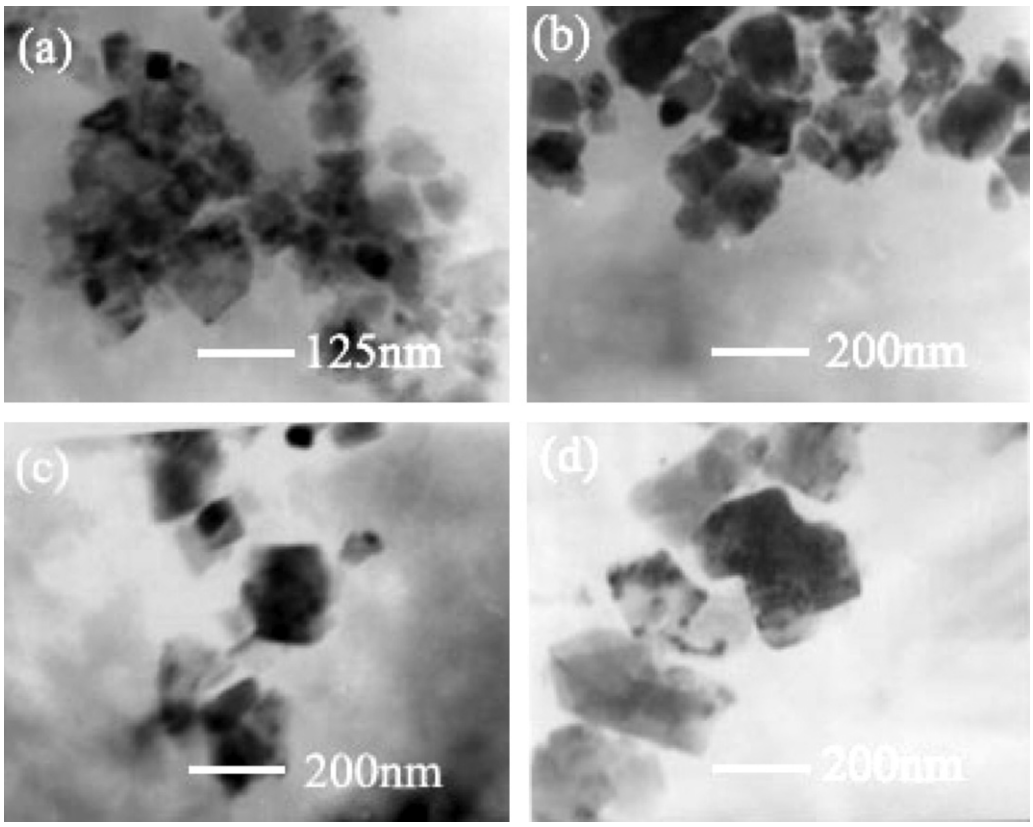

Fig. 6. Transmission electron microscopy micrographs of the NKNS-3.75LT powders obtained by heat-treating the gel at different temperatures: (a) 500 °C, (b) 600 °C, (c) 700 °C and (d) 800 °C.

is accompanied by a reduced degree of agglomeration. Considering the balance between the particle growth and agglomeration, it would be appropriate to calcine the gel powder at 600 °C in this study.

The SEM images of the sol–gel derived NKNS-3.75LT ceramics sintered at various temperatures are shown in Fig. 7. Noticeably, the sample density obviously increases with increasing the sintering temperature but the phenomenon of abnormal grain growth (AGG) can be observed as the sintering temperature rises to 1070 °C. With a further increase of sintering temperature, the sample becomes denser and the grain size tends to become more and more homogeneous such that a bimodal distribution of the grain size slowly dies away, indicating that normal grain growth (NGG) starts. Simultaneously the average grain size becomes large with increasing the sintering temperature as expected. When the sintering temperature increases to 1130 °C, the grain size looks uniform and but gets significantly coarsened, leading to a slight reduction of the density. The special grain growth behavior with an increase of sintering temperature has been recognized in some NKN-based ceramics manufactured by solid state reaction methods [30,31]. For perovskites, AGG has been explained by faceting, in connection with attachment sites for growth such as dislocations or polytype stacking faults favoring a small number of grains in an otherwise blocked matrix of small grains [32,33]. This explanation fits to the faceted grain morphology of NKNS-3.75LT particles (see Fig. 6). Moreover, both Park and Shen suggested that the change of grain growth behavior from AGG to NGG be correlated with the existence of liquid phases owing to the volatilization of Na_2O [31] or the excess of Na_2O [34]. However, yet the formation mechanism of liquid phases seems to be not very clear. We thought that the specific particle morphology of polyhedron could also facilitate the formation of liquid phases at sharp-angled contacts between particles at higher sintering temperatures. As the sintering temperature is relatively low (density is also low), the liquid phases formed only at locally existed particle contacts leads to the rapid growth of a small amount of particles (AGG). As the sintering temperature increases, the number of particle contact becomes much more such that the formed liquid phase tends to be more uniformly distributed, and thereby more grains could nucleate and then normally grow simultaneously. This mechanism of forming liquid phases correlated to locally higher contact pressure could be as a supplement to the existing explanation about AGG, although more supports from experiments are needed in future. On the other hand, it can be seen that the samples look still porous as sintered at 1050 °C but the grain size has reached the submicron scale. The fast grain growth tends to weaken the driving force of densification, which often happens in a conventional pressure-less sintering of nano-scaled powders with high surface free energies. The optimal temperature of 1090 °C, at which the highest density of 4.63 g/cm^3 can be obtained, was only slightly decreased compared to that in previous works [8], which could be correlated with the existing soft agglomeration of powders and even the shaping method of green compacts. The study on whether it can be improved using cold-isostatic pressing is still in progress.

The physical and various electrical properties of sol–gel derived and conventionally processed NKNS-3.75LT ceramics were summarized in Table 1 for comparison. It is obvious that the optimum sintering temperature and the corresponding grain size in this study were slightly reduced compared to those of samples by a mixed oxide method. The sol–gel derived NKNS-3.75LT ceramics sintered at 1070 °C have huge grains (5 μm) and small grains (1 μm), typical of the abnormal grain growth. The normal grain growth starts to disappear with further increasing temperature and then the average grain size is ~2 μm. The sol–gel derived

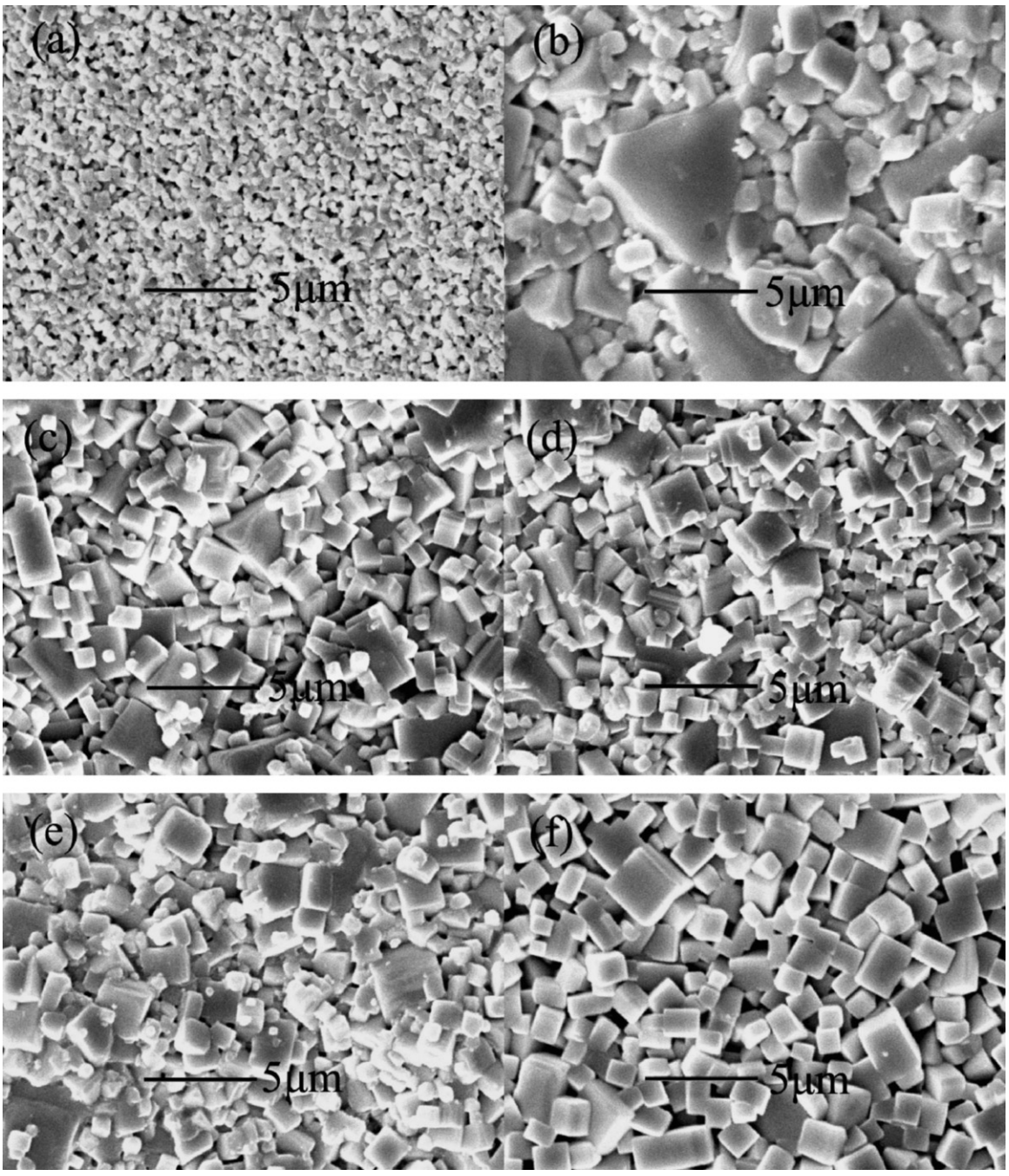

Fig. 7. Scanning electron microscopy micrographs of sol–gel derived NKNS-3.75LT ceramics sintered at different temperatures: (a) 1050 °C, (b) 1070 °C, (c) 1080 °C, (d) 1090 °C, (e) 1110 °C and (f) 1130 °C.

Table 1
Sintering behavior and electrical properties of NKNS-3.75LT ceramics prepared by different processing methods.

Processing	Sintering temperature (°C)	Density (g/cm^3)	Average grain size (μm)	P_r ($\mu C/cm^2$)	d_{33} (pC/N)	k_p	ε_{33}^T	tanδ	T_c (°C)
Mixed oxide method [8]	1100	4.62	2.5	20.8	395	0.52	2390	0.04	251
Modified sol–gel	1070	4.39	1 or 5	–	323	0.46	1992	0.039	258
method [this study]	1090	4.63	2	25.6	418	0.54	2413	0.037	257
	1110	4.56	2.7	24.1	332	0.48	2296	0.045	261

NKN-3.75LT, $(Na_{0.52}K_{0.4425})(Nb_{0.8825}Sb_{0.08})O_3-0.0375LiTaO_3$.

ceramics sintered at 1090 °C exhibit improved densification and attractive dielectric, ferroelectric and piezoelectric properties of $\rho = 4.63\ g/cm^3$, $\varepsilon_{33}^T = 2413$, $\tan\delta = 0.037$, $P_r = 25.6\ \mu C/cm^2$, $d_{33} = 418\ pC/N$ and $k_p = 0.54$ in addition to similar T_c values (257 °C), compared to those prepared by mixed oxide methods, demonstrating that the citrate sol–gel method could be advantageous for making high-performance lead-free piezoelectric ceramics. The high chemical homogeneity and relatively high sintering activity would be helpful for systems with complex compositions and difficulties in sintering.

4. Conclusions

A modified sol–gel processing route to synthesize NKNS-3.75LT nano-scaled powders (30–100 nm) was investigated using Nb_2O_5 and Ta_2O_5 as niobium and tantalum to replace costly metal alkoxides. TG-DSC and XRD measurements along with FT-IR and Raman analysis indicated that citric acid was successfully chelated with metal ions to form a stable network, and that the complete crystallization of the NKNS-3.75LT powder started at 500–600 °C, significantly lower than that for a mixed-oxide route. The sol–gel derived ceramics sintered at 1090 °C have dense fine microstructures and excellent electrical properties of $d_{33} \sim 418\ pC/N$, $k_p \sim 0.54$, $\varepsilon_{33}^T \sim 2413$, $T_c \sim 257$ °C, demonstrating a tremendous potential of this method for making high-performance lead-free ceramics.

Acknowledgements

This work was financially supported by Key Project of Natural Science Research of Universities in Anhui Province (KJ2009A089), a project of Natural Science Foundation of Anhui Province (090414179), National Natural Science Foundation of China (50972035), and a Program for New Century Excellent Talents in University, State Education Ministry (NCET-08-0766).

References

[1] L. Egerton, D.M. Dillon, J. Am. Ceram. Soc. 42 (1959) 438.
[2] R.Z. Zuo, J. Rodel, R.Z. Chen, L.T. Li, J. Am. Ceram. Soc. 89 (2006) 2010.
[3] S.J. Zhang, R. Xia, T.R. Shrout, Appl. Phys. Lett. 91 (2007) 132913.
[4] C.W. Ahn, C.S. Park, C.H. Choi, S. Nahm, M.J. Yoo, H.G. Lee, S. Priya, J. Am. Ceram. Soc. 92 (2009) 2033.
[5] Y. Saito, H. Takao, T. Tani, T. Nonoyama, K. Takatori, T. Homma, T. Nagaya, M. Nakamura, Nature 432 (2004) 84.
[6] E. Hollenstein, M. Davis, D. Damjanovic, N. Setter, Appl. Phys. Lett. 87 (2005) 182905.
[7] B.Q. Ming, J.F. Wang, P. Qi, G.Z. Zang, J. Appl. Phys. 101 (2007) 054103.
[8] R.Z. Zuo, J. Fu, D.Y. Lv, J. Am. Ceram. Soc. 92 (2009) 283.
[9] T.A. Skidmore, T.P. Comyn, S.J. Milne, Appl. Phys. Lett. 94 (2009) 222902.
[10] Y.L. Wang, D. Damjanovic, N. Klein, E. Hollenstein, N. Setter, J. Am. Ceram. Soc. 90 (2007) 3485.
[11] T. Rojac, A. Benčan, H. Uršič, B. Malič, M. Kosec, J. Am. Ceram. Soc. 91 (2008) 3789.
[12] Q. Xu, X.L. Chen, W. Chen, S.T. Chen, B. Kim, J. Lee, Mater. Lett. 59 (2005) 2437.
[13] M.L. Zhao, C.L. Wang, J.F. Wang, H.C. Chen, L.W. Zhong, Acta Phys. Sinca 53 (2004) 2357.
[14] P. Pookmanee, G. Rujijanagul, S. Ananta, B. Robert, S. Heimann, Phanichphant, J. Eur. Ceram. Soc. 24 (2004) 517.
[15] X. Jing, Y. Li, Q. Yin, Mater. Sci. Eng. B 99 (2003) 506.
[16] H.A.M. van Hal, W.A. Groen, S. Maassen, W.C. Keur, J. Eur. Ceram. Soc. 21 (2001) 1689.
[17] J.G. Hou, Y.F. Qu, W.B. Ma, D. Shan, J. Mater. Sci. 42 (2007) 6787.
[18] E. Mercadelli, C. Galassi, A.L. Costa, S. Albonetti, A. Sanson, J. Sol–Gel Sci. Technol. 46 (2008) 39.
[19] F. Soderlind, P.O. Kall, U. Helmersson, J. Cryst. Growth 281 (2005) 468–474.
[20] K. Tanaka, K. Kakimoto, H. Ohsato, J. Cryst. Growth 294 (2006) 209.
[21] F.P. Lai, J.F. Li, Z.X. Zhu, Y. Xu, J. Appl. Phys. 106 (2009) 064101.
[22] A. Chowdhury, J. Bould, Y.F. Zhang, C. James, S. J. Milne, J. Nanopart. Res., doi:10.1007/s11051-009-9595-0.
[23] C. Wang, Y.D. Hou, H.Y. Ge, M.K. Zhu, H. Yan, J. Eur. Ceram. Soc. 29 (2009) 2589.
[24] H.Q. Wang, R.Z. Zuo, L. Wang, J. Fang, X.H. Wang, L.T. Li, J. Mater. Sci. Mater. Electron. doi:10.1007/s10854-010-0159-y.
[25] A. Reisman, F. Holtzberg, J. Am. Chem. Soc. 77 (1955) 2115.
[26] H.Q. Wang, R.Z. Zuo, Y. Liu, J. Fu, J. Mater. Sci. 45 (2010) 3677.
[27] B. Stuart, Infrared Spectroscopy: Fundamentals and Applications, John Wiley and Sons Ltd., 2004.
[28] M. Vivekanandhan, M. Venkateswarlu, N. Satyanarayana, Mater. Lett. 58 (2004) 1218.
[29] X.H. Zeng, Y.Y. Liu, X.Y. Wang, W.C. Yin, L. Wang, H.X. Guo, Mater. Chem. Phys. 77 (2002) 209.
[30] K. Kakimoto, K. Akao, Y.P. Guo, H. Ohsato, Jpn. J. Appl. Phys. 44 (2005) 7064.
[31] H.Y. Park, C.W. Ahn, H.C. Song, J.H. Lee, S. Nahm, K. Uchino, H.G. Lee, H.J. Lee, Appl. Phys. Lett. 89 (2006) 062906.
[32] J.G. Fisher, S.J. Kang, J. Eur. Ceram. Soc. 29 (2009) 2581.
[33] M. Bäurer, S.J. Shih, C. Bishop, M.P. Harmer, D. Cockayne, M.J. Hoffmann, Acta Mater. 58 (2010) 290.
[34] Z.Y. Shen, Y.H. Zhen, K. Wang, J.F. Li, J. Am. Ceram. Soc. 92 (2009) 1748.